APPROXIMATE EFFECTS OF OFF-CENTER ACOUSTIC SONDES AND ELLIPTIC BOREHOLES UPON FULL WAVEFORM LOGS

by

M.E. Willis, M.N. Toksöz and C.H. Cheng

Earth Resources Laboratory
Department of Earth and Planetary Sciences
Massachusetts Institute of Technology
Cambridge, MA 02139

ABSTRACT

Full waveform acoustic well logging has become instrumental to hydrocarbon exploration because of its ability to determine in situ velocity information for P and S waves as well as the attenuation (or absorption) of seismic energy. It is therefore important that the factors influencing these logs be understood. In addition to formation properities, Poisson's ratio, the borehole environment, and tool centering can affect the full waveform acoustic logs. These latter factors are evaluated through modeling of elliptic boreholes and de-centralized tools in the borehole.

INTRODUCTION

A number of factors affect the observed full waveform acoustic log amplitudes. Formation properities play an important role. In addition the borehole environment can cause variations. For example, borehole rugosity impedes the propagation of head waves (Morris et al., 1964). In areas of cavitation and washouts, critical refraction may be prevented, resulting in low amplitude waveforms. Lebreton et al. (1978) report a strong reduction in waveform amplitude proportional to an increase in mud cake thickness.

Centering of the sonde and a cylindrical borehole are crucial to waveform amplitudes and arrival times. In most full waveform logging systems the tool is held centralized in the borehole by several bow type springs which press against the formation. In other systems, rubber "fingers" keep the tool centralized. The reliability of these methods in keeping the tool centralized in holes with a true circular cross section as well as in irregular holes has not been well documented. The actual amount of "rattle" that the tool experiences is not generally known.

Morris estimates that moving the source one quarter of an inch (0.64 cm) off-center decreases the P wave amplitude by one half (Morris et al., 1964). This is a significant effect for such a small displacement. In experiments with a tool placed in a trough to simulate a cased borehole it was determined that moving the centralized source completely against the casing not only decreases the amplitude of the recorded waveform but also increases its complexity and reverses the apparent polarity of the first motion (Riddle, 1962). Studies by Forristall and Ingram (1969) show that an off-centered condition for a fluid cylinder yields two types of reflected arrivals: one associated with the source waveform, and the other with its derivative.

Roever et al. (1974) conclude that when the source and detector are displaced off-center on the same side, P waves constructively interfere, and S waves destructively interfere, and that when source and detector are on opposite sides of the center, P waves destructively interfere while S waves constructively interfere. Approximations for P and S waves for an off-center source in terms of a sum of an infinite number of potentials have been derived by Winbow (1980).

Non-circular cross section boreholes may be due to washouts, abrasion of the drill string against the borehole wall, or by the release of local stresses around the borehole. Certainly in soft formations the first two effects are dominant. Irregular cross sections are difficult to model accurately without resorting to numerical methods. The interest of this paper lies in the qualitative effect of a non-circular borehole. For this reason an elliptic borehole is examined. Strain relaxation around the borehole results in elliptic deformation of the borehole and it is possible that drill string abrasion could results in an elliptic borehole cross section as well.

In this paper the terms "off-center" and "tilted" have specific meanings. A tool is off-center when it is located off the central axis of the borehole in one radial direction and remain parallel to the axis of the borehole. A tool is tilted when it has an arbitrary tilt with respect to the hole geometry.

MODELS OF ELLIPTIC BOREHOLES AND DECENTRALIZED TOOLS

Three simple approximate modeling techniques and one exact method are presented to offer new insight into the borehole irregularity problem. The first assumes that the waveforms may be summed from intermediate sized boreholes to approximate the elliptic and off-center cases. The second method uses a high frequency assumption to perform ray tracing of critically refracted body waves (i.e., P and S headwaves) for a tilted sonde. The third method uses a Huygen-type wavefront analysis to check the validity of the other two methods. For a special case with the source on borehole axis the effect of moving the receiver off the axis is modeled. Finally, a statistical approach is discussed to remove the ellipticity effects of the hole and tilt of the sonde from the recorded waveforms.

Elliptic Borehole

The first model assumes that the sonde is located on the central axis of a borehole with an elliptic cross section and eccentricity ε, as shown in Figure 1. Each ray which leaves the source will encounter the wall of the borehole at a different radial distance away from the sonde. This distance, r_e, is the effective radius of the borehole for that particular take off angle. φ is the take off angle, in plan view, of each ray as it leaves the source, referenced from the shortest ray path as shown in Figure 1. For a zero take off angle (φ=0) the ray "sees" a small borehole. For each larger take off angle the ray "sees" a progressively larger borehole until $\varphi=\frac{\pi}{2}$ where it "sees" the largest borehole. It is assumed that for each take off angle around the source the propagation path of the waveform can be isolated. This waveform is replaced by a waveform from a centered sonde in a circular borehole with the corresponding effective borehole radius, r_e, for that particular take off angle. Each take off angle is replaced with a waveform from a centered sonde in a circular borehole with this technique. The sum of these waveforms is a stacked waveform which approximates the log from an elliptic borehole. It is not feasible to analyze all

take off angles, a representative number of them are evaluated.

The method developed by Cheng and Toksöz (1981) to generate synthetic acoustic waveforms for the borehole is used to model the off center case. While their method does not contain a tool in the hole, they show that an effective tool radius can be subtracted from the borehole radius to match actual waveforms. A borehole radius of 4 inches (10.2 cm) and an effective tool radius of 1.36 inches (3.5 cm) is used for all cases studied. An effective attenuation with Q = 35 (see Cheng and Toksöz, 1981) has also been included. The effective attenuation is essentially an exponentially decaying envelope applied to the waveform to simulate attenuation. The borehole is divided into sixteen equally spaced regions around the source. Since the problem is symmetric in φ four take off angles can be used in the quarter circle with φ=11.25°, 33.75°, 56.25°, 78.75° to model these sixteen regions. It has been assumed that the source is axially symmetric so that the equally spaced waveforms will carry the same weight in the summation.

It is obvious that washouts and bridging may cause highly non-circular holes which could radically alter the character of the full waveform logs. It is not clear whether the relaxation of local stresses through the deformation of the borehole could effect a measurable change in the waveforms.

Figure 2 shows a synthetic seismogram generated for a centered tool in a limestone formation with parameters listed in Table 1. Clearly visible are the a) P, b) leaky (or PL) mode, c) pseudo-Rayleigh, and d) Stoneley waves, and e) the Airy phase of the pseudo-Rayleigh wave.

An estimate of a relatively high value of strain release for a 4 inch (10.2 cm) radius borehole at normal logging depths is needed. Parameters for the two rock types modeled, the Bedford limestone and the Chico siltstone, were obtained from Birch (1966). Young's modulus, E in megabars, and Poisson's ratio, υ, for each rock are shown in Table 1. An order of magnitude estimate of regional stresses at a depth of 8.2 kft (2.5 km) was obtained from McGar and Gay (1978, Figure 5). The horizontal stresses for this model, σ_x and σ_y, should be less than 1 kbar. Accordingly, the sum of the horizontal stress, $\sigma_x+\sigma_y$, is less than 2 kbar, and the stress difference, $\sigma_x-\sigma_y$, is less than 1 kbar. The estimates of the properties of regional stresses were related to the strain release through an equation derived by Jaeger and Cook (1979, equation 15.3(2)). The minimum and maximum relative deformations are $\xi(\Sigma-\delta)$ and $\xi(\Sigma+\delta)$, respectively,

$$\text{where } \xi=\frac{R(1+\upsilon)}{2E}$$

$$\Sigma=\sigma_x+\sigma_y$$

$$\delta=(\sigma_x-\sigma_y)(3-4\upsilon)$$

R is the radius of the borehole, and the other parameters are as before. Also listed in Table 2 are the strain releases found for each rock.

The maximum relative deformation is 0.087 inches (2.21 mm). In order to determine a reasonably high upper limit for the effects of stress relaxation or a minor amount of hole deterioration, a synthetic seismogram was generated for an elliptic borehole with a relative deformation of 0.16 inches (4.06 mm) using the summing method above. The parameters used to generate this synthetic waveform are shown in Figure 3 and listed in Table 1.

It can be seen that there is indeed a large effect upon the log even from this small amount of ellipticity. These effects can be classified into several observations about the elliptic log relative to the centered log: 1) the P wave arrival remains intact, 2) the PL waves are reduced in amplitude, 3) the S wave arrival remains intact, 4) the pseudo-Rayleigh wave is reduced after the shear arrival (due to the highly dispersive nature of its phase velocity), 5) the Stoneley wave is preserved, and 6) the Airy phase of the pseudo-Rayleigh wave is preserved. While it may not be possible in general to separate the local stress relaxation from the general borehole condition it is important to note that small changes in the borehole shape can produce large effects in the observed waveforms.

Off-Center Tool in a Circular Borehole

The second model assumes that the sonde is located off-center in one direction radially by an amount br, where r = radius of the borehole, as shown in Figure 4. This places the sonde parallel to the central axis of the borehole. Each ray which leaves the source will encounter the wall of the borehole at a different radial distance away from the sonde. As before, this distance, r_e, is defined as the effective radius of the borehole for that particular take off angle. Figure 4 shows φ, the take off angle, in plan view of each ray as it leaves the source. In this geometry, when φ=0, the ray "sees" a small borehole. For each larger take off angle the ray "sees" a progressively larger borehole until $\varphi=\pi$ where it "sees" the largest borehole. The assumption is made that for each take off angle around the source we can isolate that portion of the propagation path. It will be replaced by a waveform from a centered sonde in a borehole with the corresponding effective borehole radius for that particular take off angle. As before, by summing up a representative number of these waveforms a stacked waveform is generated which approximates the log from an off-center sonde.

The same borehole radius, effective tool radius, and the same effective attenuation value is used for this model as with the elliptic model. Here the borehole has been divided into eight equally spaced regions around the source. Since the problem is symmetric in φ four take off angles can be used in the half circle with φ=22.5°, 67.5°, 112.5°, 157.5° to model these eight regions. Again, it is assumed that the source is axially symmetric so that the equally spaced waveforms will carry the same weight in the summation.

Figure 5a shows a summed synthetic waveform approximating a 5% (.2 inch or 5.08 mm) off-center sonde for the limestone formation as before. Figure 5b shows a 10% (0.4 inch or 10.2 mm) model. The reduction in amplitude is greater for the off-center than for the elliptic model but the waveforms are effected in the same general manner.

We generated synthetic waveforms for sandstone (Figure 6) and for shale (Figure 7) both centered and 10% off-center. The formation properties for these units are also listed in Table 1. Similar interference effects can be seen on these examples as well.

Frequency Effect

The synthetic seismograms generated contain all the wave types present which interact in complicated ways. A larger borehole radius can produce multiple reflections as well as higher modes of the pseudo-Rayleigh wave. The P wave cannot be easily separated from the leaky mode, nor the S wave from the pseudo-Rayleigh wave. In order to determine the frequency dependence of this

summing method upon headwaves for the off-center model a smearing operator was applied after a method proposed by by Morris et al. (1964) and Huntley (1968). This operator simulates the effect of the different arrival times at the receiver for the same headwave as it propagates down the borehole. The ray which takes off with $\varphi=0$ arrives earlier than the ray which leaves with $\varphi=\pi$. The duration, T_0, of the operator is given by

$$T_0=\frac{4br\cos(\gamma)}{V_m} \tag{1}$$

where γ = the critical angle of refraction ($\gamma=\arcsin\frac{V_m}{V_f}$), V_m = borehole fluid velocity, and V_f = formation velocity. If the smearing operator, $s(t)$, is convolved with a headwave from a centered sonde, $c(t)$,

$$o(t)=s(t)*c(t) \tag{2}$$

the off-centered headwave $o(t)$, from this model should be simulated. By studying the amplitude spectrum of the smearing operator, a prediction of its effect on the headwaves can be made.

In order to construct this operator, the relative travel time as a function of take off angle must be determined. This is the travel time for an off-centered headwave relative to its travel time for the centered case. Figure 8 shows an example of a travel time curve for a limestone formation with formation properties listed in Table 1. Since this is a symmetric problem only positive angles of φ have been plotted. The left hand scale shows the total travel time for a 10% off-center sonde. The right hand scale shows this travel time relative to a headwave from a centered tool in the same formation. For a zero take off angle the travel time is faster (and hence is negative or earlier) than the centered case since the distance is shorter. For $\varphi=\pi$ the travel time is longer.

To convert this travel time information into a measure of the number of rays arriving at the receiver as a function of time, it is assumed that the source is axially symmetric and equal angles about the source contain an equal amount of energy. In addition, it is assumed that the energy of each ray is concentrated at its arrival time. Taking equal time intervals, starting with the earliest arrival time, the amplitude of the energy arriving in each interval is proportional to the change in φ in that time interval. Analytically, the operator $s(t)$ is given by

$$s(t)=\frac{1}{2\pi}\sum\frac{d\varphi}{dt} \tag{3}$$

where the sum is taken over all contributions of $\frac{d\varphi}{dt}$, at time t, of the multi-valued function $\varphi(t)$. It is easy to see that for the degenerate case, i.e., a centered tool, the smearing operator is (and must be) $\delta(t)$, the Kronecker delta function. For extrema and inflection points of non-trivial $t(\varphi)$ curves, $t\frac{d\varphi}{dt}$ is proportional to $\delta(t)$. At these points Airy phase type contributions exist. For computational ease $s(t)$, is discretized to $s(n\Delta t)$. In order to approximate $\frac{d\varphi}{dt}$, we numerically differentiate $\varphi(t)$ in the following manner. ΔT is defined as the difference between the maximum and minimum travel times, t_{max} and t_{min}, respectively. ΔT is divided into N equal time increments, Δt. $s(n\Delta t)$ is then:

$$s(n\Delta t) = \begin{cases} 0 & \text{for } n\Delta t < t_{min} \\ \frac{1}{2\pi\Delta t} \sum_{\varphi^*} |\varphi((n+\frac{1}{2})\Delta t) - \varphi((n-\frac{1}{2})\Delta t)| & \text{for } n\Delta t \text{ otherwise} \\ 0 & \text{for } n\Delta t > t_{max} \end{cases} \quad (4)$$

where again, the sum is taken over all φ^* of the multi-valued function $\varphi(t)$, with contributions in the time interval $(n-\frac{1}{2})\Delta t$ to $(n+\frac{1}{2})\Delta t$. If Δt is increased by decreasing N, we add more smoothing to the delta function contributions at extrema and inflection points. The predominant effect of the smoothing is to reduce the high frequencies. At logging frequencies, approximately 10-20 kHz, the main contribution of the smearing operator to the full waveform log comes from its period, ΔT. The details of its exact shape, i.e., the "spikiness" of the delta function contributions, generally affect the higher frequencies which are above the bandwidth of most tools.

Figure 9 shows a set of smearing functions for limestone when the sonde is between 1% and 11% off-center. The time axis is given for time relative to the centered headwave arrival time. Table 1 lists the properties for these cases. Figure 10 shows the amplitude spectra for the smearing functions for limestone, sandstone, and shale P waves. From these spectra it can be predicted, for example, that for a limestone with a 40 kHz source 3% (.12 inch or 3.05 mm) off-center, the reduction in P headwave amplitude would be 13%.

Ray Tracing Model

A simple ray tracing technique is utilized to model headwaves generated by an off-center source in the borehole. The results of this method provide insight and understanding of the complexity of the problem. A rigorous adherence to the results, however, requires a higher frequency source than is commonly used. The model allows the sonde to be positioned to tilt in any arbitrary fashion within the borehole. Snell's law is strictly applied at the source end of the tool but must be relaxed somewhat at the receiver end. In the cylindrical geometry critical refraction paths from the source to the wall can be uniquely defined. What is relatively surprising, however, is that the only rays which propagate straight down the wall are those with take off angles of zero and π. All other ray paths contain varying amounts of spin or helical bending around the borehole. The spin angle, Δ, measured from the vertical, can be determined from simple geometry and Snell's law as

$$\tan\Delta = \frac{b\sin\vartheta}{\left(\frac{(1-b\cos\vartheta)^2}{\cos^2\gamma} - 1 - b^2 + 2b\cos\vartheta\right)^{\frac{1}{2}}} \quad (5)$$

where ϑ = the take off angle of the source measured relative to the center of the borehole as shown in Figure 11, with b and γ the same as before.

In general when these rays are traced from the wall to the receiver they will not critically refract back to the receiver location due to their spin. Snell's law is therefore relaxed by neglecting the spin angle in computing its refraction path back to the receiver.

The ray paths for all take off angles can be computed for this model. It is easiest to display these ray paths on a flat surface which represents the cylindrical wall of the borehole. One edge of the borehole is "cut" in the z direction and unrolled to lie flat. It is a similar type projection as that used for

the borehole televiewer data. On this display which in this paper is termed the unwrapped borehole projection, the ray paths in the fluid cannot be seen but the critically refracted rays on the wall are easily seen. It is convenient to circumferentially extend the display in a periodic fashion in order to show rays which spin around the borehole. This will alleviate bookkeeping when a ray "falls" off the edge of one side of the display and must be brought back on again to the other side as it spins completely around the borehole.

Figure 12 shows the unwrapped borehole for the limestone previously studied with a 10% off-center sonde. The two lines at about z=.033 feet (0.01 m) and 7.94 feet (2.42 m) which extend in the $r\vartheta$ direction show the location of all critical refracted rays which hit the wall from the source and where the rays refract back from the wall to the receiver, respectively. The many lines extending between these points are some of the individual ray paths on the wall.

Once the ray paths are determined, the travel time for these rays can be computed. Figure 13 is the travel time curve for the same limestone as Figure 12. The plot shows travel time vertically as a function of take-off angle, φ, from the source. This travel time changes as shown in Figure 14 if the top of the tool is held as before and the bottom of the tool is moved so that it is located at z=8 feet (2.44 m), r=0.033 feet (0.0102 m), and $\vartheta=-\pi$. This makes the bottom of the tool 10% off center in the other direction. The character of the resulting travel time curve is changed significantly. There is a reduction in total travel time and the $\varphi=0$ direction is no longer the fastest path.

As before, these travel time curves can be changed into a time series representing the smearing function and analyzed in the frequency domain to estimate their effect on the spectral content of centered headwaves. Figure 15a shows the amplitude spectra for a limestone formation with 3% off-center source at three distances, z=8, 12 and 20 feet (2.44, 3.66, and 6.10 meters). The reduction of headwave amplitude appears more severe with distance. Figure 15b shows the amplitude spectra for the previous three rock types with source/receiver separation of 8 feet (2.44 meters) and a source 3% off-center. The effect is more severe at the slower velocities. Figure 15c shows the same case as Figure 15b with the tool tilted so that the receiver is at z=8 feet (2.44 meters), $\vartheta=-\pi$. The effect at this distance is not as great as in the former case. The results of this method are in fairly close agreement with those obtained by the summing method for small values of sonde off centeredness and tilt.

Wavefront Analysis

A wavefront analysis technique has been implemented to check the validity of the results obtained through ray tracing. Each critically refracted ray is assumed to act as a Huygen's point source for headwaves on the wall. The critically refracted rays are easily determined from Snell's law as before. When a ray hits the wall of the borehole it begins a point source of headwaves. This is represented by a circular wavefront emanating from the point at which the ray hit the wall. As time progresses the circular wavefront travels out from the point source. The interaction of the circular wavefronts from all of the rays delineates the actual front of the headwave. "Snap-shots" of the headwave front at any desired time can be taken using this technique. Figure 16 shows a sequence of snap-shots of the wavefront for a sandstone formation 1% off-center. The straight lines are the rays determined by the ray tracing method above. The circular wavefronts for each point source may appear distorted due to the exaggeration between the depth, z, and the $r\vartheta$ axes. A comparison of the

accuracy of the ray tracing method with the wavefront analysis method shows, in general, that the ray tracing overestimates the duration of the smearing operator by between 10 and 20%. This results in an amplitude spectrum with reduced estimates of the true spectral values. The wavefront analysis could be extended to model the off-center perturbations more accurately.

TILTED TOOL

Tsang and Rader (1979) have formulated the pressure response for an azimuthally symmetric borehole. The source is located on axis and the receiver can be placed off-axis. The receiver can be thought of as a ring pressure transducer. Since the wavefield is symmetric, however, the ring receiver response is the same as an off-axis point receiver.

Synthetic waveforms can be generated exactly for a centralized source and an off-axis receiver. This is a special case of the tilted tool model described above. The formulations for body wave attenuation (Cheng et al., 1982) and a Ricker wavelet source (Ricker, 1944) time shifted to appear more causal (Willis, 1983) are used to generate these synthetic waveforms. Figure 17 shows a limestone model with parameters listed in Table 1. These parameters are similar to those in Figures 2 and 5. Figure 18 shows a sandstone model similar to that in Figure 6. Figure 18 shows the shale model we presented in Figure 7. Again, the parameters are listed in Table 1. The same general trends as before are observable in these exact models. The main difference is that the effect is not as pronounced. The receiver must be placed farther off-axis before the effect is as dramatic as with the summing method.

DISCUSSION

Techniques have been presented to estimate the sensitivity of the full wave acoustic waveforms to borehole asymmetries and tool positioning. At present, these estimates may be used in a qualitative manner. Results of this study indicate the need for a more thorough investigation.

Most studies of full waveform acoustic logs compare the travel time differences and amplitude ratios of the waves recorded at two or more receivers. The travel time differences and amplitude ratios are most strongly affected by off-centering and tilting that results from the differences between the receiver locations. Only the total effect from source to receiver and not the difference between two receivers has been examined in this study.

Several trends have been observed as a result of this investigation. Asymmetries and tool positioning have a larger effect on higher frequencies than on low frequencies. The size of the ringing P wave packet decreases as does the central portion of the pseudo-Rayleigh wave with an asymmetrical tool position while the Stoneley wave is relatively unaffected.

At the present time it is not possible to directly measure the positioning of the sonde in the borehole. If the amplitude of a particular phase is needed, for example, to obtain the attenuation Q_p^{-1} or Q_s^{-1}, the tilt of the tool and the borehole ellipticity must be known to correct for these effects. Utilization of a multiple arm caliper tool could provide the borehole ellipticity information. Tool tilt could be determined through "reverse profiling" as in standard surface refraction seismology. Most presently available tool configurations, however, are limited to single direction measurement. Alternatively, a statistical approach can be applied to currently available data. Summing many waveforms

(or spectra of waveforms) results in a biased estimate of the waveform at that depth interval. The bias would depend (at least in part) upon the average amount of borehole ellipticity and tool tilt in the distance it traveled. If a reasonable estimate of these quantities can be obtained, corrections could eliminate most of the bias in the spectral amplitudes. In addition, an adaptive filter can be constructed to remove these effects from the stacked waveforms. Since the amount of tilt possible is related to the length of the tool and the positions of the receivers, the estimated tilt correction will be a function of each tool design, receiver location, and the annular radius between the tool and the borehole wall. Therefore, for a given tool configuration and depth interval to be studied, a correction filter can be constructed for the waveforms from each source/receiver pair.

TABLE 1—Model Parameters

Figure	Velocities (km/s) V_p	V_s	Densities (g/cc) Rock	Z (m)	b (% off-center)
2	5.94	3.05	2.3	2.44	0
3	"	"	"	"	*
5a	"	"	"	"	5
5b	"	"	"	"	10
5c	"	"	"	"	20
6a	4.27	2.44	2.14	"	0
6b	"	"	"	"	10
7a	3.20	1.83	2.0	"	0
7b	"	"	"	"	10
8	5.94		"	10	
9	"			"	1-11
10a	"			"	1-11
10b	4.27			"	1-11
10c	3.20			"	1-11
12	5.94			"	10 off-center
13	"			"	"
14	5.94			"	10 tilted
15a	"			2.44 3.66 6.10	3 off-center
15b	" 4.27 3.20			2.44	3 off-center
15c	"			"	3 tilted
16	4.57			"	1 off-center

Note: In Figures 2-7 the effective tool radius used was 0.035m. In all cases (except Figure 3) the borehole radius was 0.102m, eccentricity = 0.27; semi-minor axis = 0.102m

TABLE 2—Relative Radial Displacements in Borehole

Rock	Young's Modulus (Mb)	Poisson's Ratio	Relative Radial Displacements (mm) Min.	Max.
Bedford ls ⊥	.334	.18	.0503	.767
Bedford ls ∥	.410	.29	−.0254	.610
Bedford ls ∥	.372	.22	−.0198	.683
Chico siltstone	.13	.12	−.2280	1.980

TABLE 3—Model Parameters for Special Case of Tilted Tool

Figure	Rock Type	Velocity (km/s) V_p	V_s	V_f	b (% offcenter)
17a	limestone	5.94	3.05	1.58	0
b					20
c					60
18a	sandstone	4.27	2.44	1.58	0
b					20
c					60
19a	shale	3.2	1.83	1.58	0
b					20
c					60

REFERENCES

Anderson, W. and Walker, T., 1961, Applications of open hole acoustic amplitude measurements: Soc. Petrol. Eng., paper 122.

Ando, T. and Itoh, T., 1973, Formation fracture detection by the sonic shear wave logging - laboratory studies: 14th Ann. SPWLA Log. Symp.

Birch, F., 1966, Compressibility; Elastic Constants: in Handbook of Physical Constants, Memoir 97, S.P. Clark, Ed., Geolog. Soc. Am., N.Y.

Cerveny, V., and Ravindra, R., 1971, Theory of seismic headwaves: University of Toronto Press, Toronto, Ont.

Cheng, C.H., and Toksöz, M.N., 1981, Elastic wave propagation in a fluid-filled borehole and synthetic acoustic logs: Geopysics, vol. 46, pp. 1042-1053.

Christensen, D.M., 1964. A theoretical analysis of wave propagation in fluid filled drill holes for the interpretation of the 3 dimensional velocity log: 5th Ann. Symp. of the S.P.W.L.A.

Forristall, G. and Ingram, J., 1969, Asymmetries in cylindrical waveguides: J. Acoust. Soc. Am., vol. 46, no. 1 (part 2), pp. 164-168.

Huntley, L.G., 1968, Factors affecting acoustic amplitude logs and their evaluation: Trans. S.P.W.L.A. 9th Ann. Logging Symp., paper G.

Jaeger, J.C. and Cook, N., 1979, Fundamentals of Rock Mechanics: Third Ed., Chapman and Hall, London.

Koerperich, E.A., 1978, Investigation of acoustic boundary waves and interference patterns as techniques for detecting fractures: J. of Petrol. Tech., vol. 30, pp. 1199-1207.

Lebreton, F., Sarda, J., Troceveme, F., and Morlier, P., 1978, Logging test in porous media to evaluate the influence of their permeability on acoustic waveforms: 19th Ann. Symp. of SPWLA.

McGarr, A. and Gay, N., 1978, State of stress in the earth's crust: Ann. Rev. Earth Planet. Sci., vol. 6, pp. 405-436.

Morris, R.L., Grime, D.R., and Arkfeld, T.E., 1964, Using compressional and shear acoustic amplitudes for the location of fractures: J. of Pet. Tech., pp. 623-532.

Paillet, F.L., 1981, A comparison of fracture characterization techniques applied to near vertical fractures in a limestone reservoir, Trans. of 22nd Ann. Logging Symp. of Soc. of Prof. Well Log Analysts, Vol. 2, pp. XX1-XX29.

Ricker, N., 1944, Wavelet functions and their polynomials: Geophysics, Vol. 6, pp. 314-323.

Riddle, G.A., 1962, Acoustic wave propagation in bonded and unbonded oil well casing: S.P.E. paper 454.

Roever, W., Rosenbaum, J., and Vining, T., 1974, Acoustic waves from an impulsive source in a fluid-filled borehole: J. Acous. Soc. Am., vol. 55, no. 6, pp. 1144-1157.

Toksöz, M.N. and Cheng, C.H., 1978, Modeling of seismic velocities in porous rocks and its application to seismic exploration: The Arabian Jrnl for Science and Eng., Special Issue, pp. 109-129.

Tsang, L. and Rader, D., 1979, Numerical evaluation of transient acoustic waveform due to a point source in a fluid-filled borehole: Geophysics, vol. 44, no. 10, pp. 1706-1720.

Walker, T., 1964, The interpretation of the fracture finder micro-seismogram log: Trans. of 5th Ann. SPWLA Log. Symp.

Willis, M. E., 1983, Seismic velocity and attenuation from full waveform acoustic logs, Ph. D. Thesis, Massachusetts Institute of Technology, Cambridge, Massachusetts.

Winbow, G.A., 1980, How to separate compressional and shear arrivals in a sonic log: Presented at the 50th Ann. Intl. Meeting S.E.G.

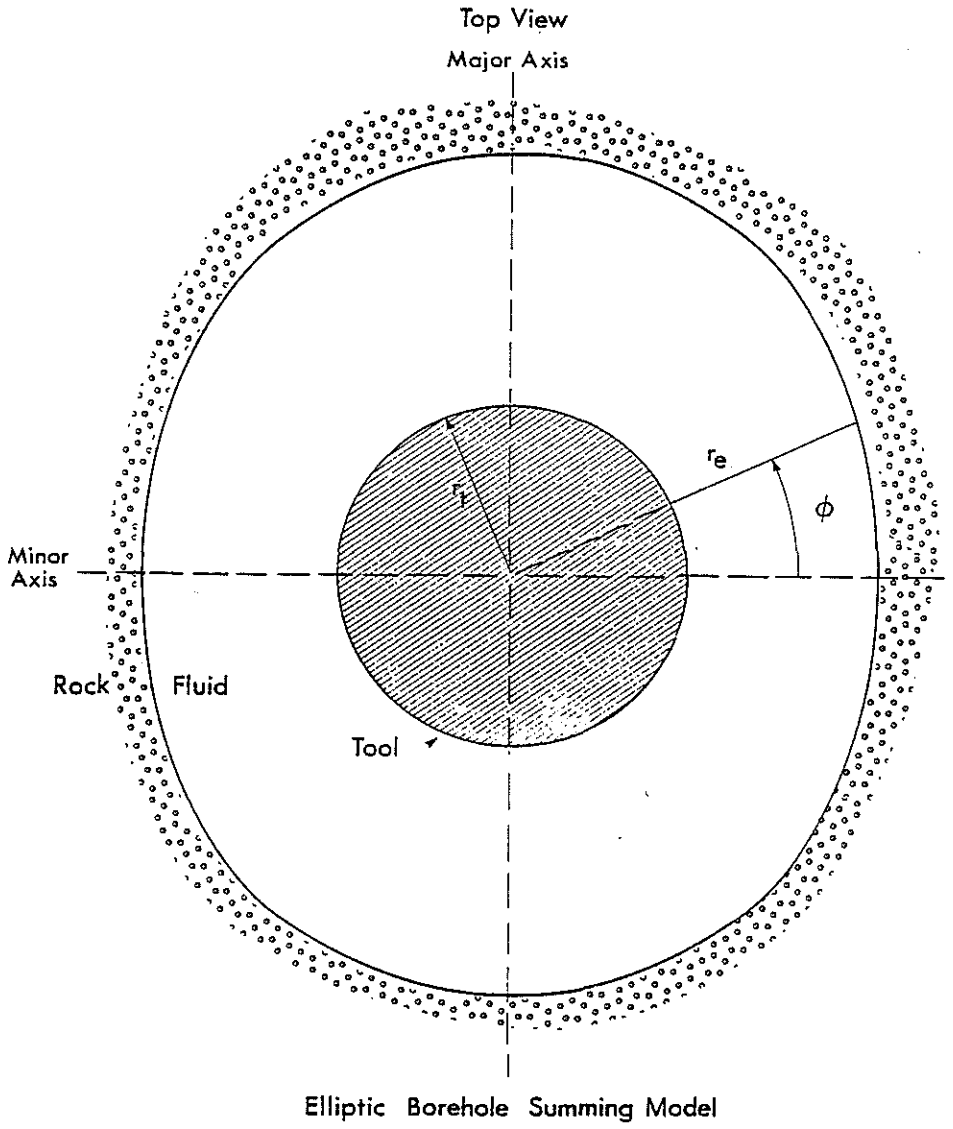

Figure 1. Schematic figure showing tool location in the borehole for the Elliptic Summing Model.

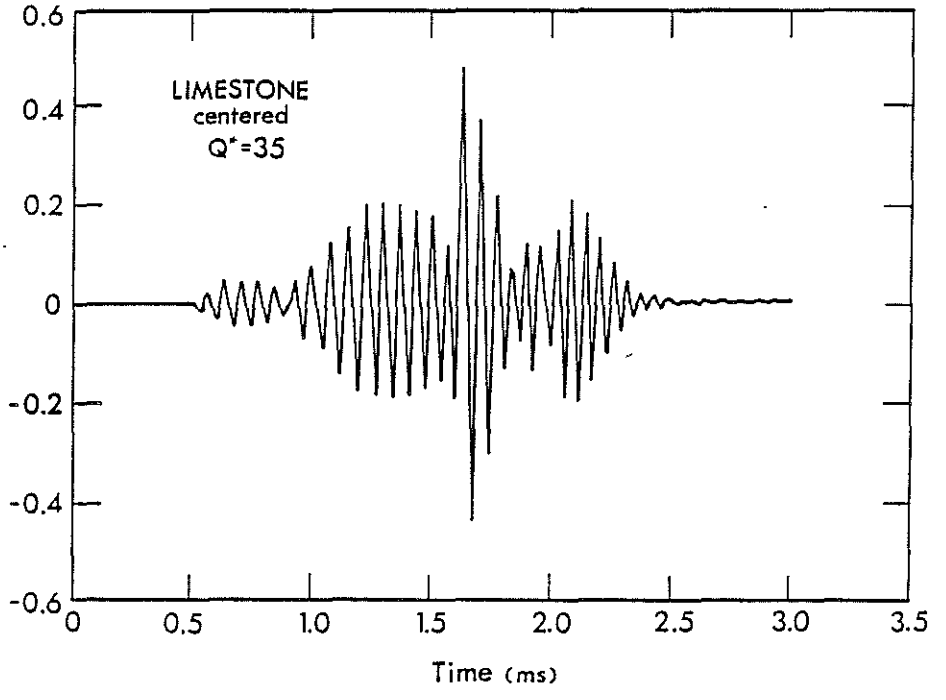

Figure 2. Synthetic waveform for a limestone formation with the tool centralized. Parameters are listed in Table 1.

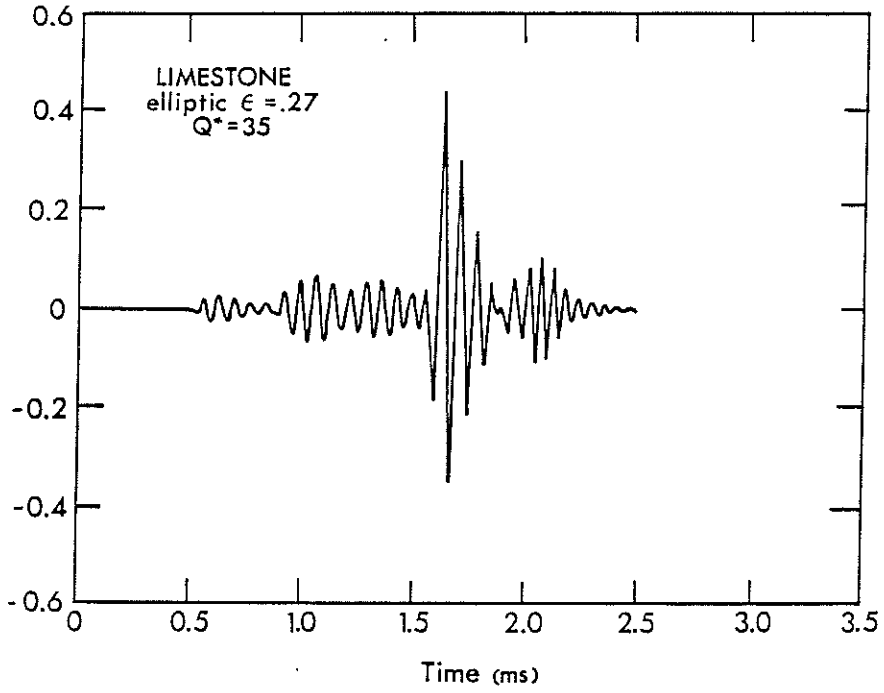

Figure 3. Synthetic waveform for a limestone formation with an elliptic borehole using the Elliptic Summing Model. Parameters are listed in Table 1.

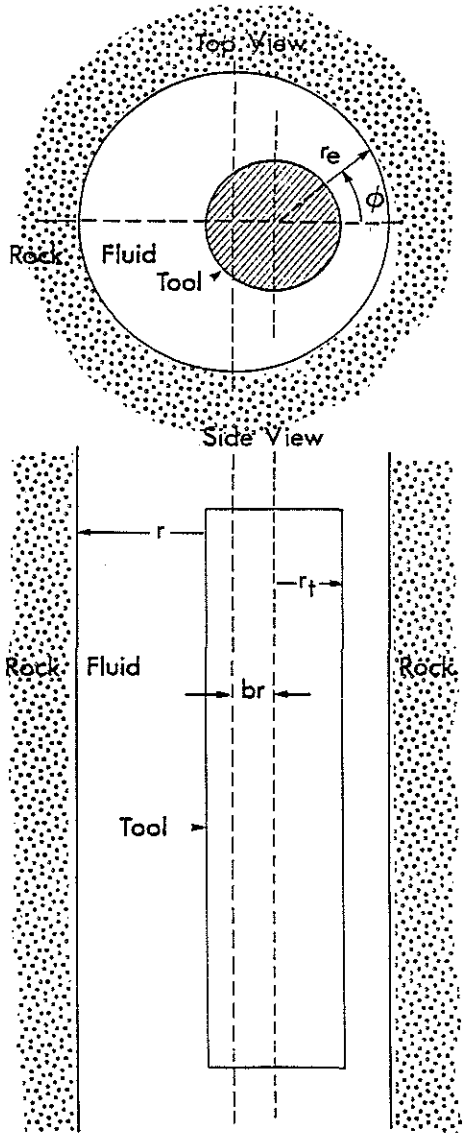

Off-Center Summing Model

Figure 4. Schematic figure showing tool location in the borehole for the Off-center Summing Model.

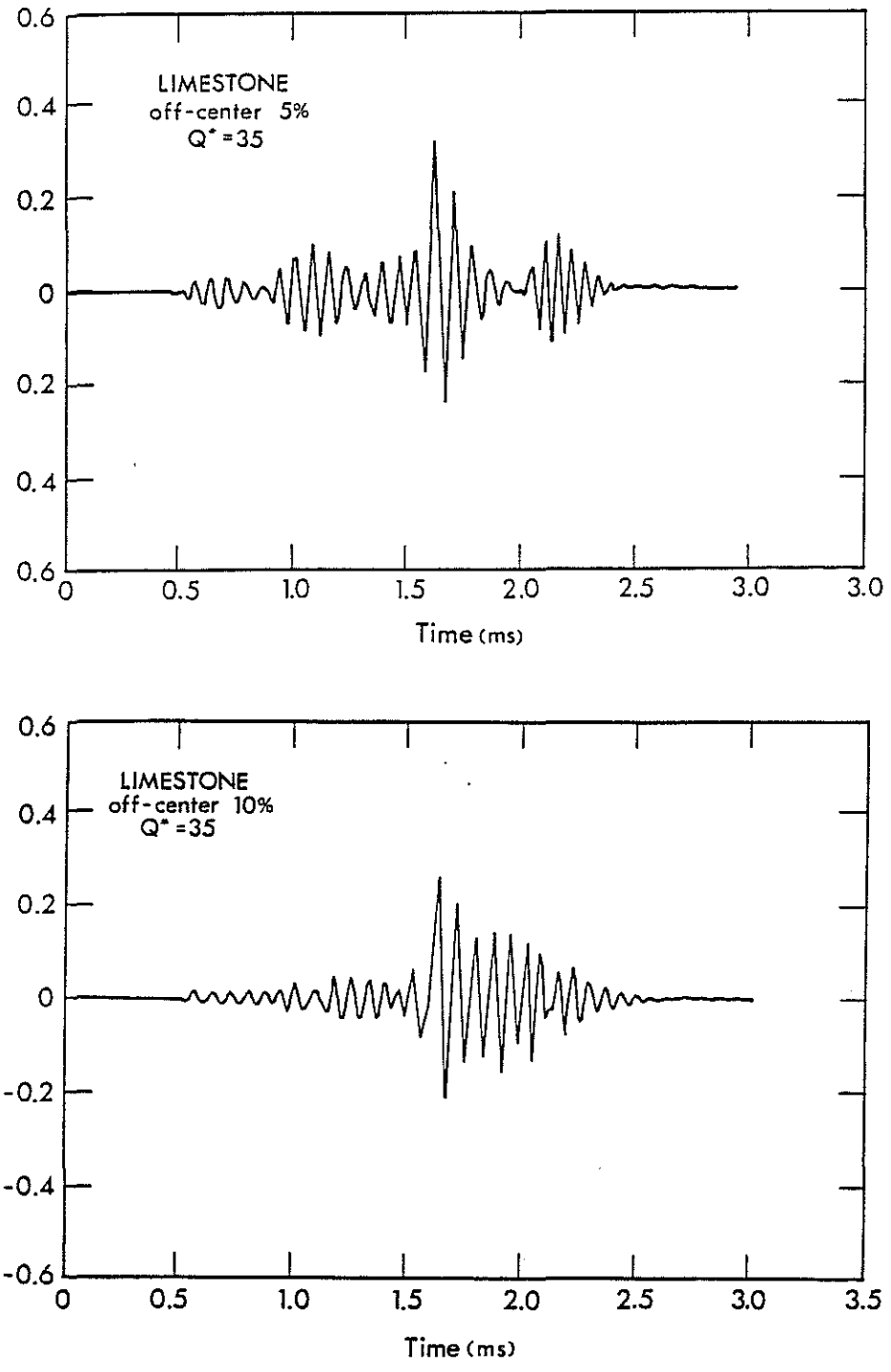

Figure 5. Synthetic waveforms for limestone formation using the Off-center Summing Method. Parameters are listed in Table 1. a) 5% off-center, b) 10% off-center.

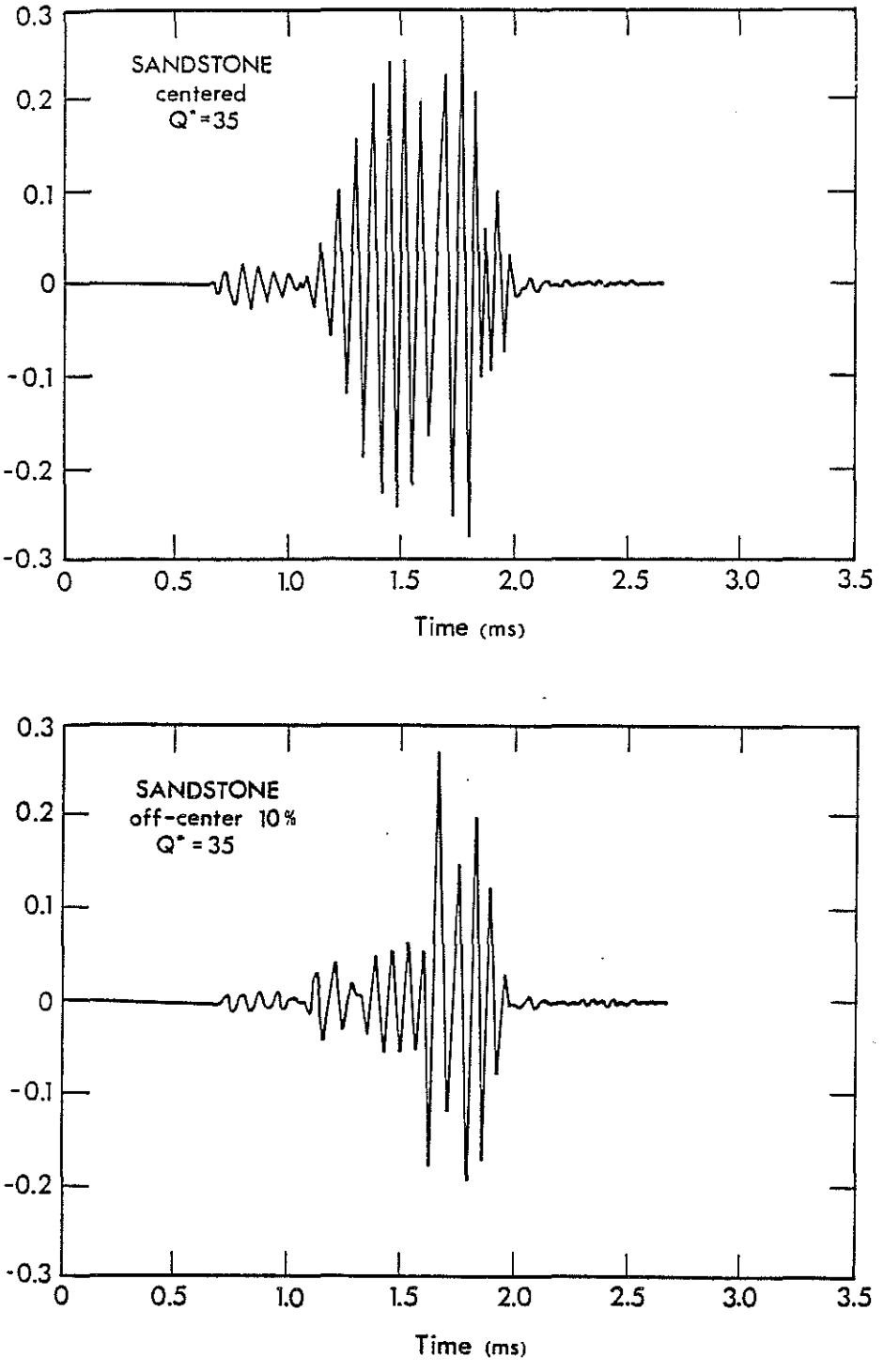

Figure 6. Synthetic waveforms for sandstone formation using the Off-center Summing Method. Parameters are listed in Table 1. a) centered, b) 10% off-center.

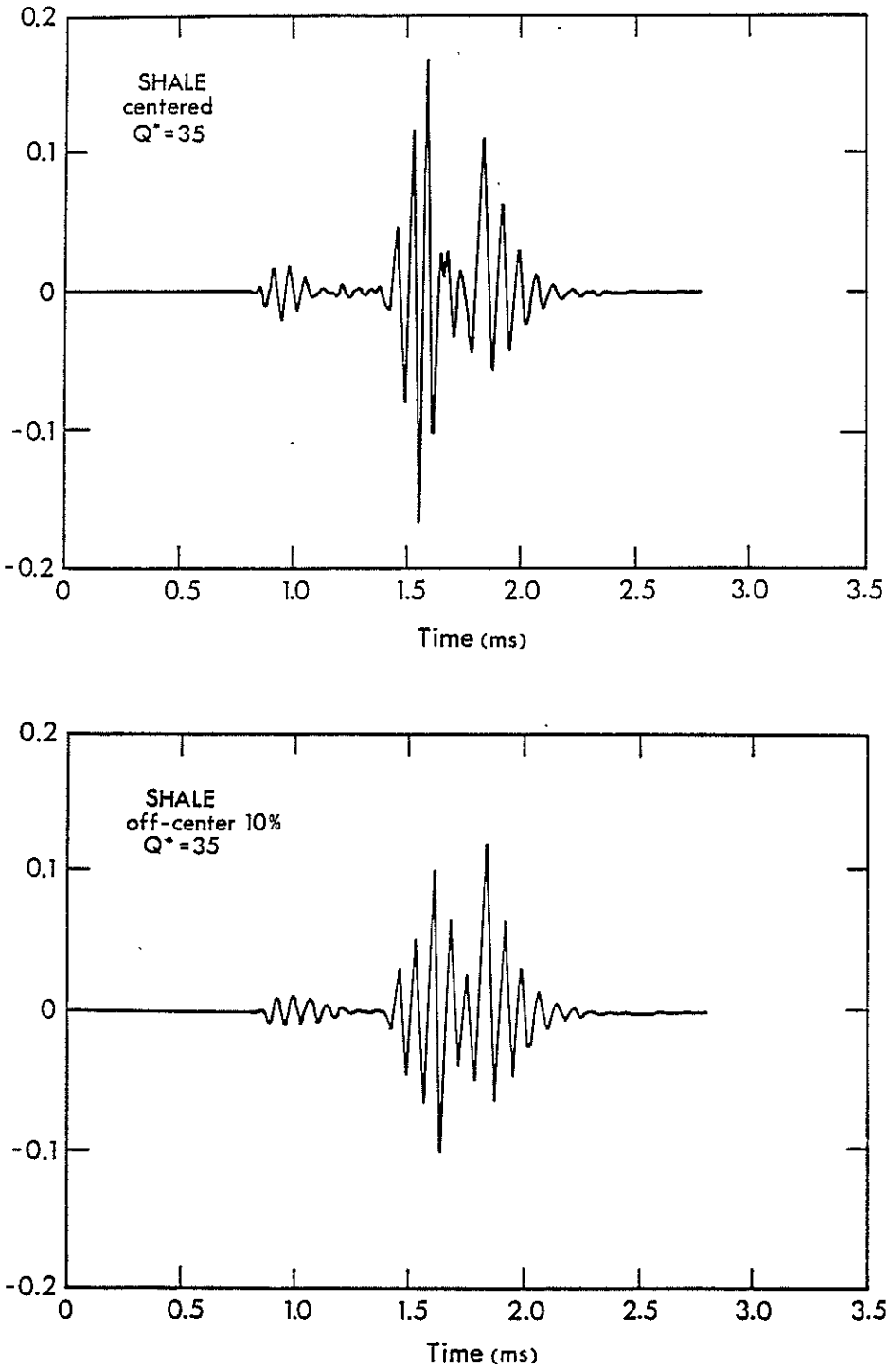

Figure 7. Synthetic waveforms for shale formation using the Off-center Summing Model. Parameters are listed in Table 1. a) centered, b) 10% off-center.

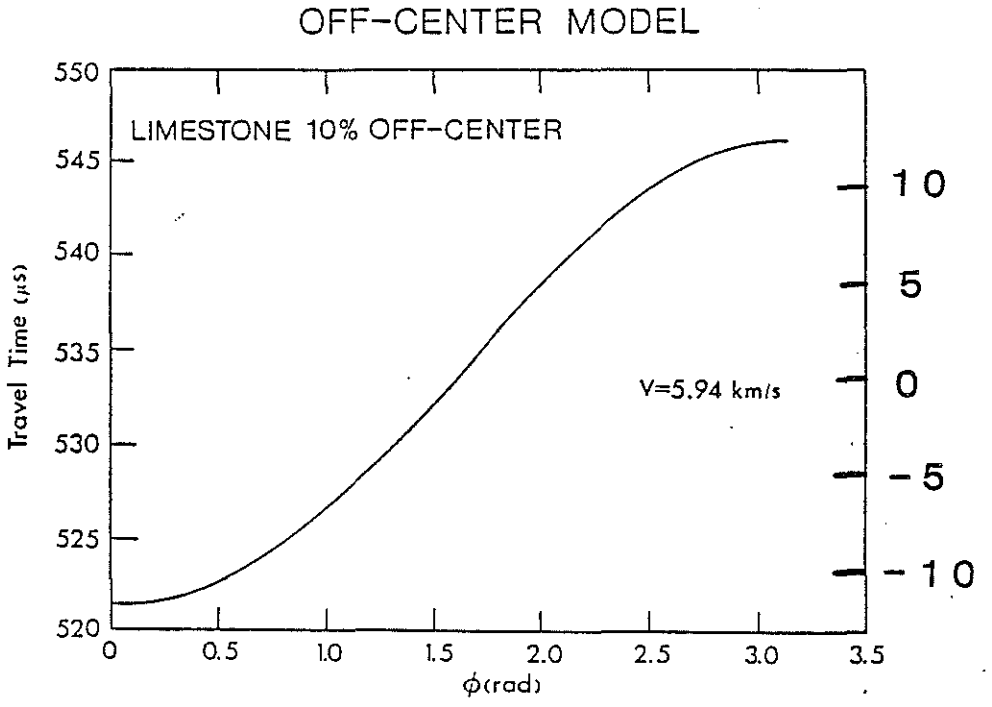

Figure 8. Off-center Summing Model travel time curve for limestone P headwaves as a function of take-off angle, φ, from the source. Parameters are listed in Table 1. Tool is 10% off-center.

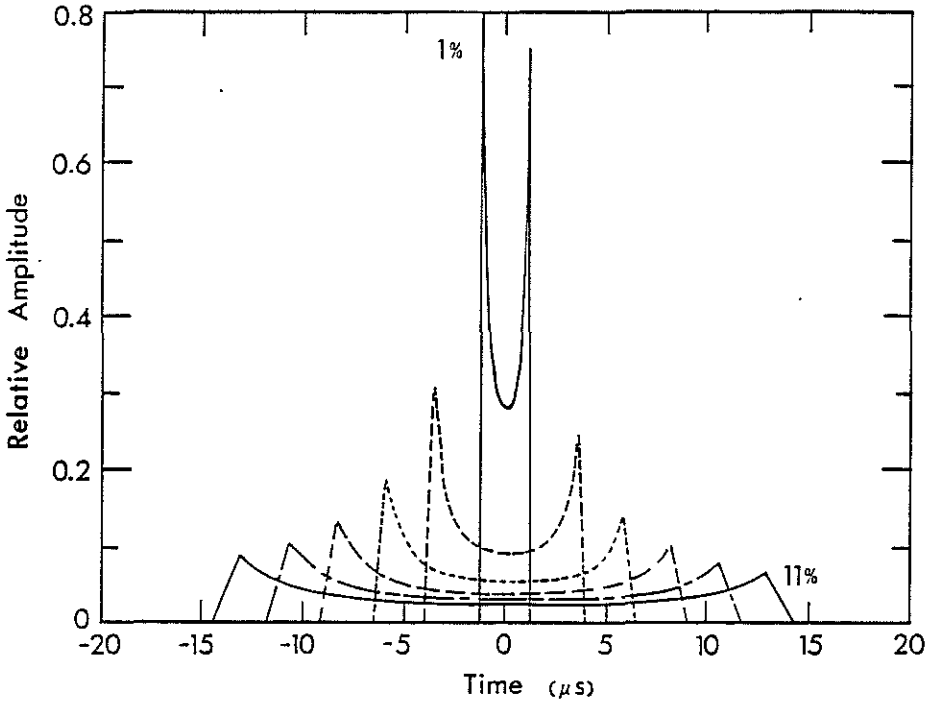

Figure 9. Off-center Summing Model smearing functions for limestone P headwaves with the tool off-center 1%, 3%, 5%, 7%, 9%, and 11%.

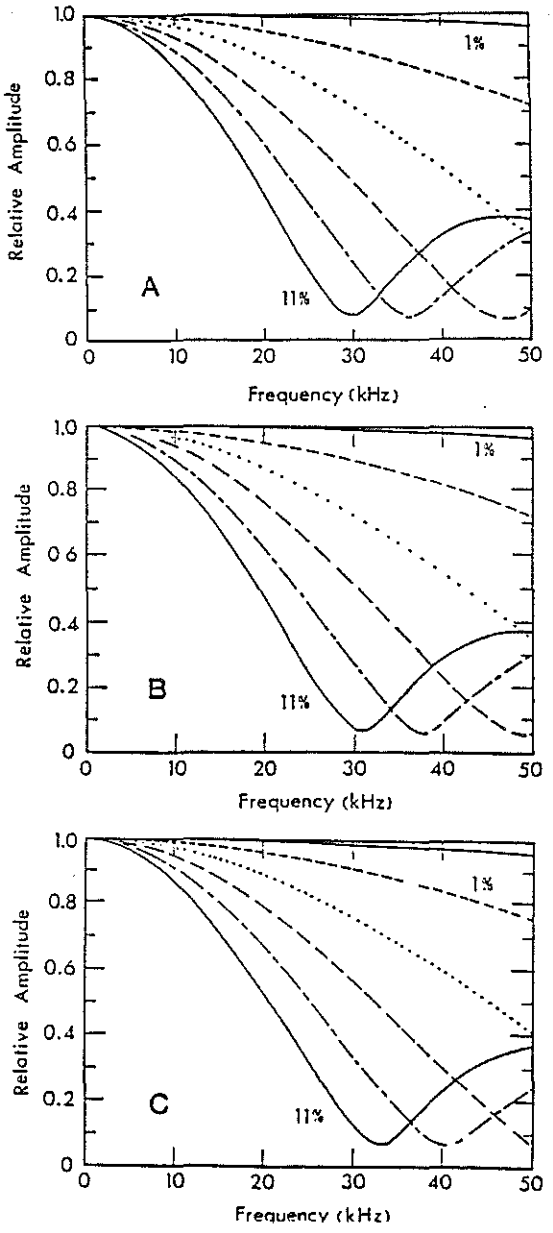

Figure 10. Amplitude spectra for the Off-center Summing Model smearing functions a) in Figure 9 for limestone, b) sandstone, and c) shale P headwaves.

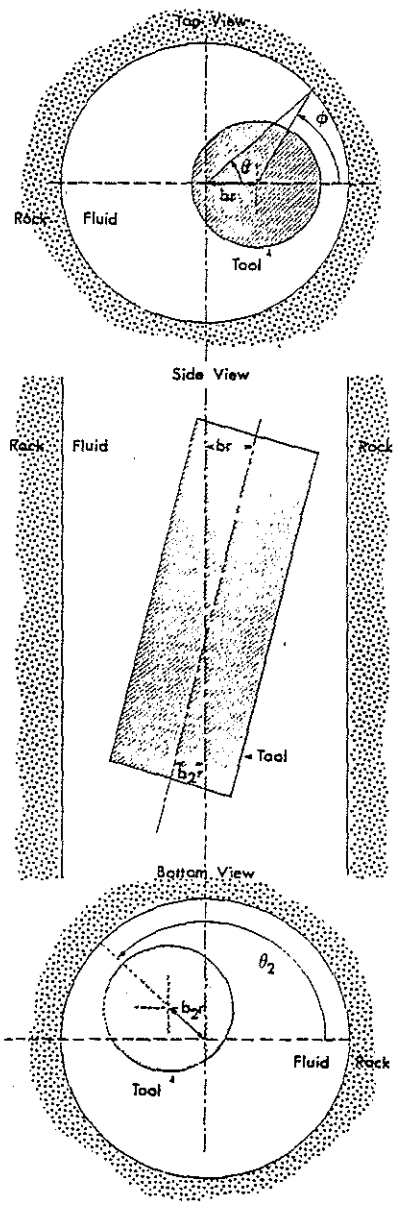

Figure 11. Schematic drawing of the ray tracing method describing the tilted sonde in the borehole.

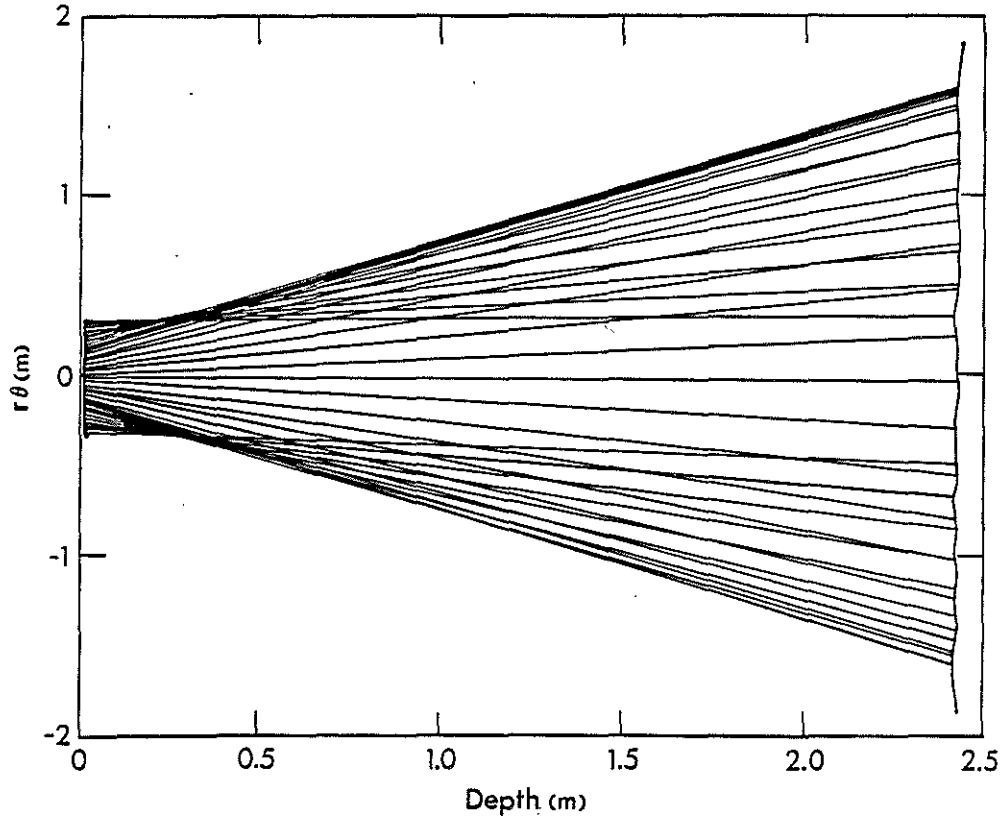

Figure 12. Unwrapped borehole projection of the ray tracing results for limestone P headwaves 10% off-center.

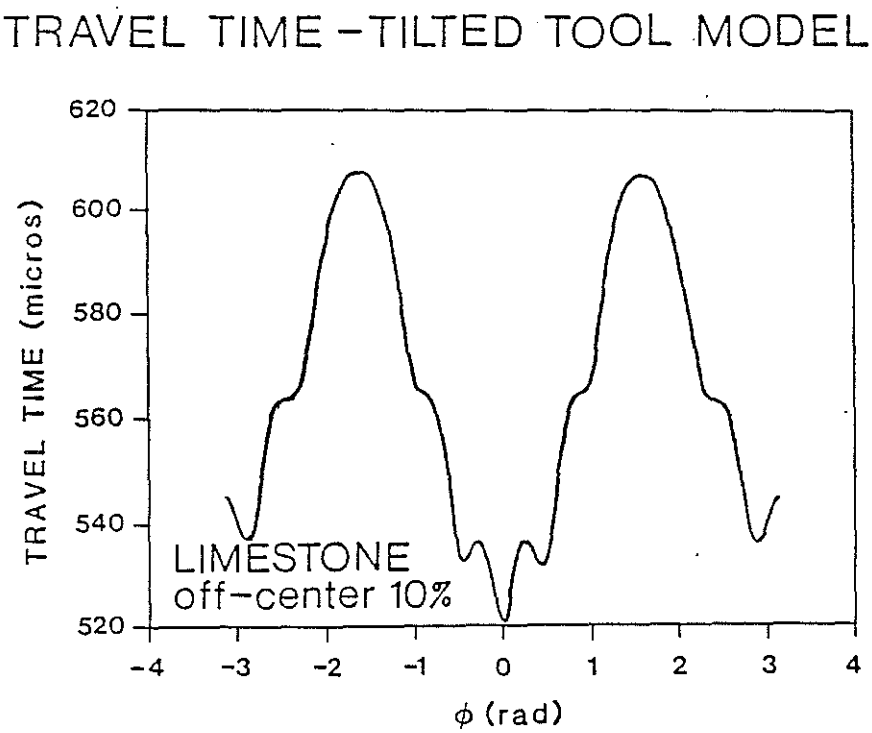

Figure 13. Ray tracing travel time curve for limestone P headwaves 10% off-center.

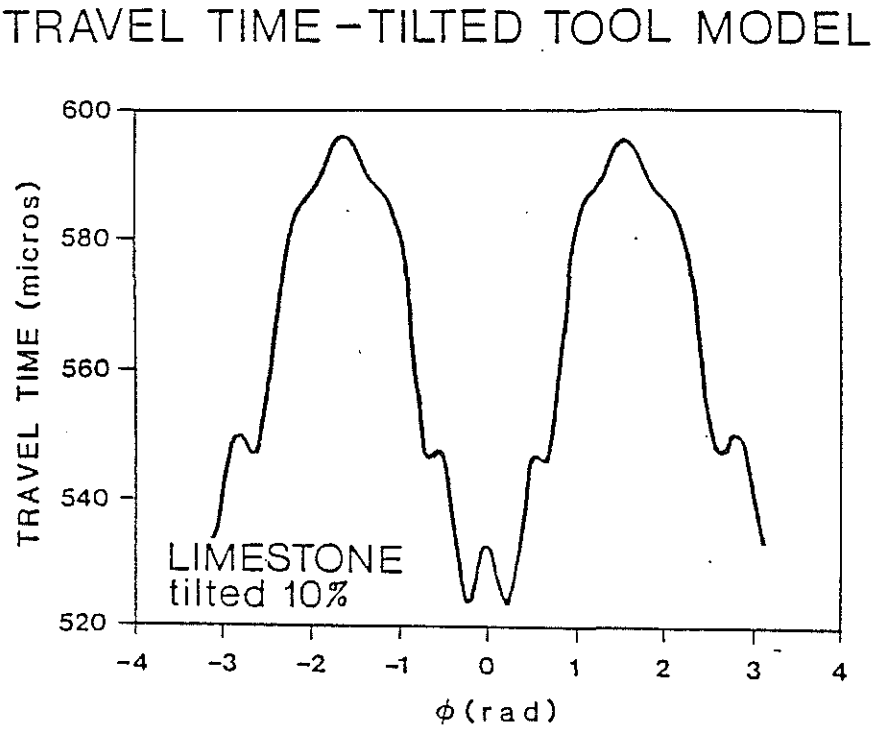

Figure 14. Ray tracing travel time curve for limestone P headwaves with the tool 10% tilted.

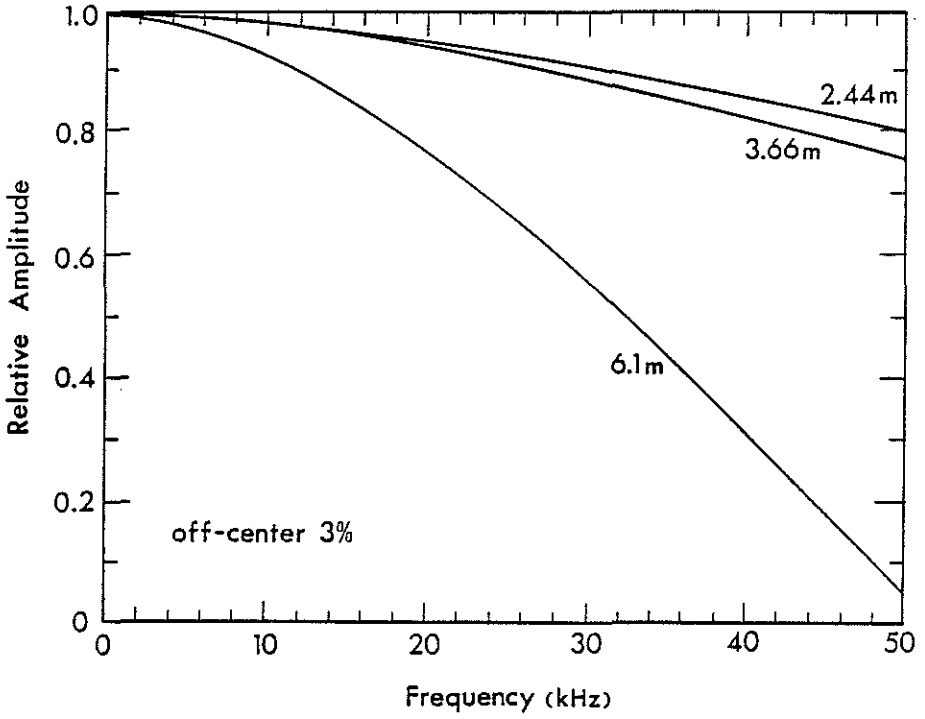

Figure 15a. Ray tracing amplitude spectra results for smearing functions for a 3% off-center limestone formation at three source/receiver distances.

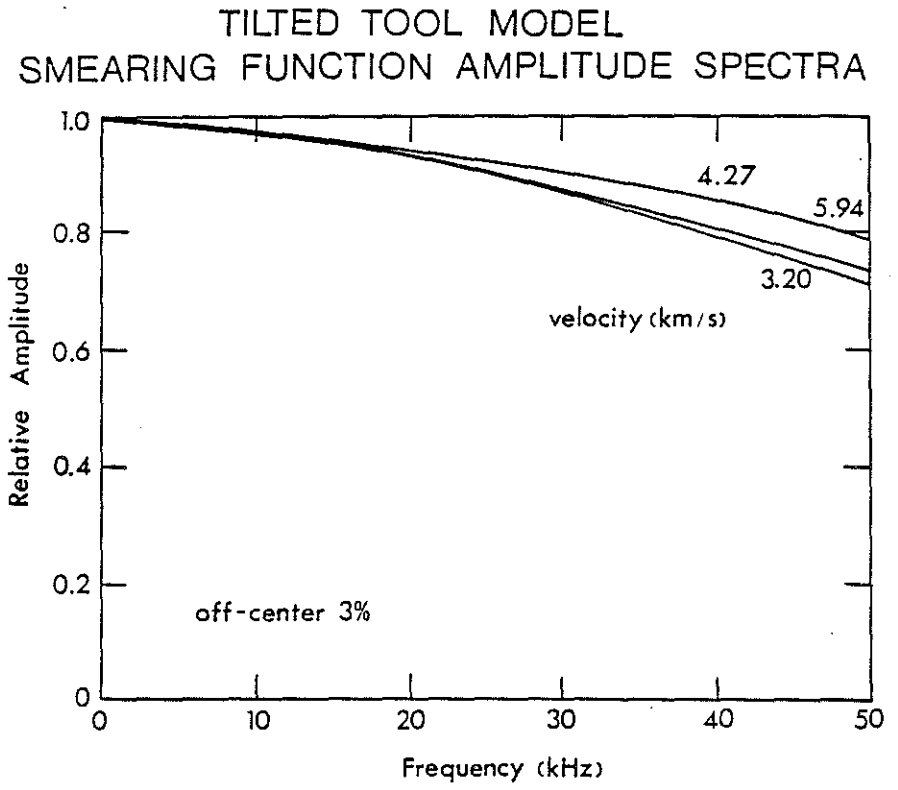

Figure 15b. 3% off-center tool for limestone, sandstone, and shale P headwaves.

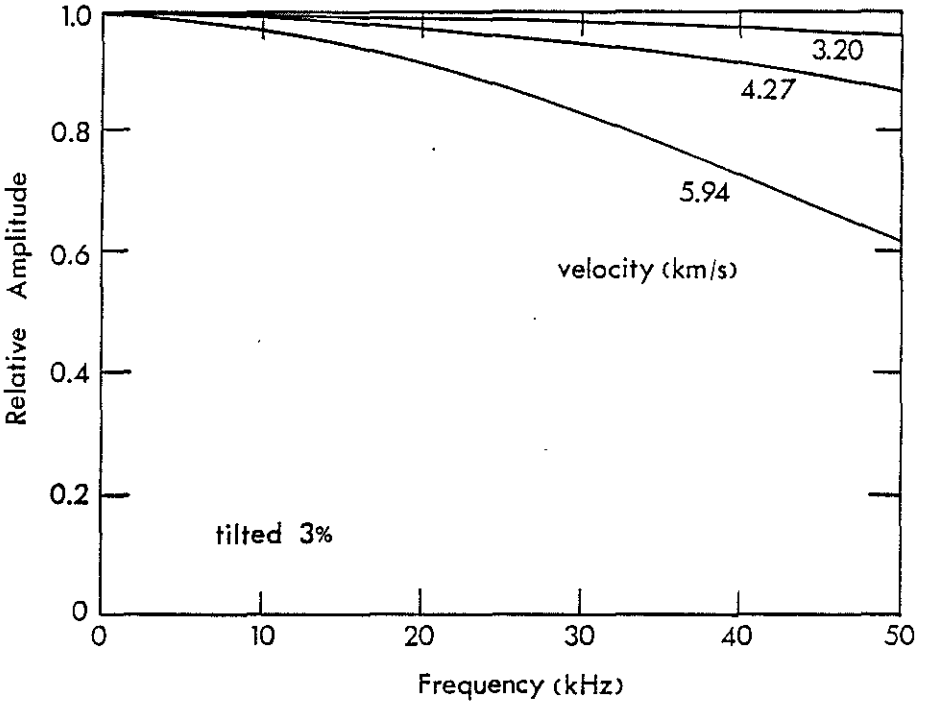

Figure 15c. 3% tilted tool for the same three formations.

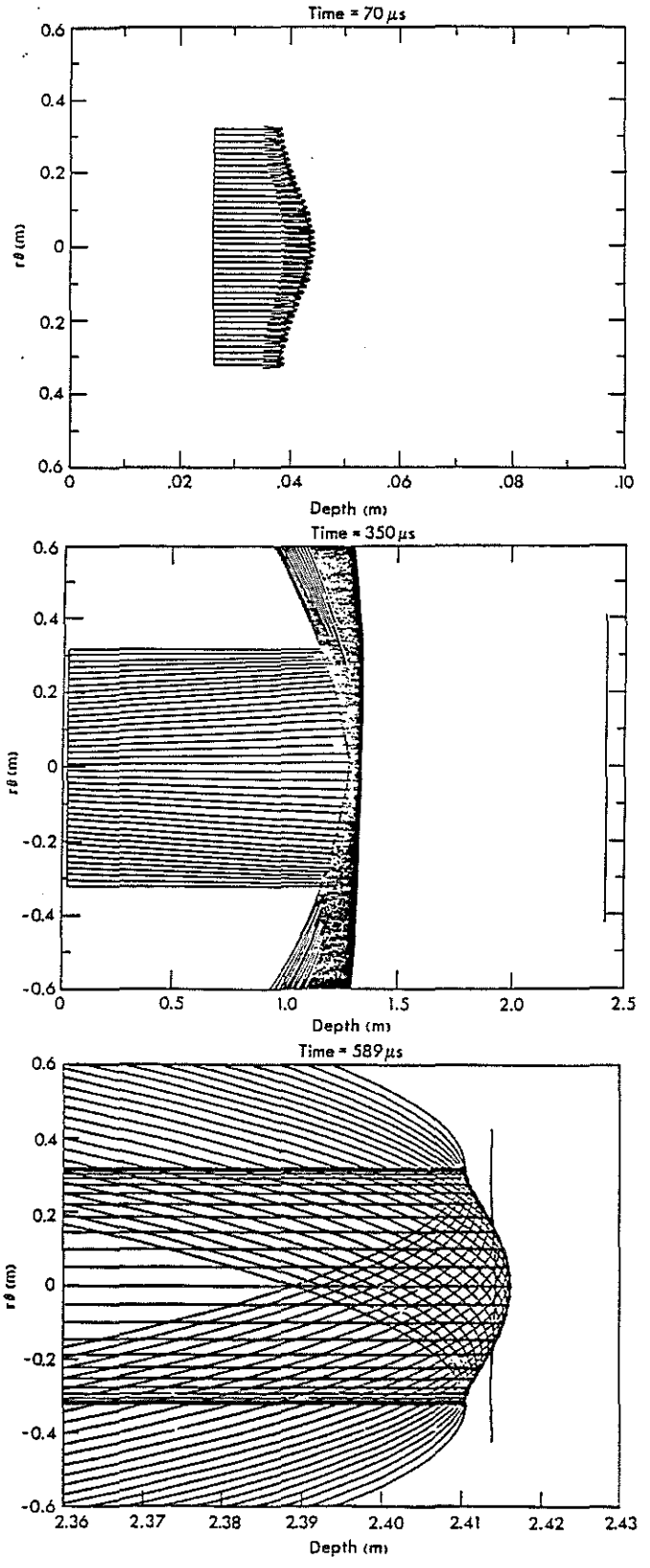

Figure 16. Wavefront analysis "snap-shots" of the unwrapped borehole projection for a sandstone with the tool 1% off-center.

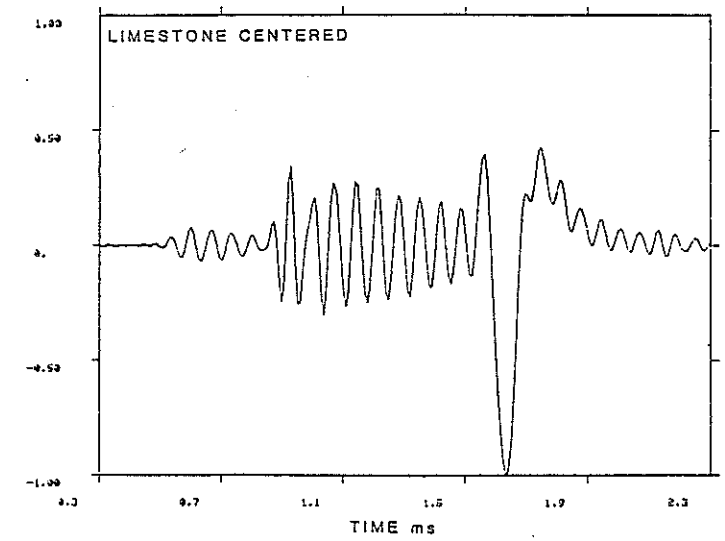

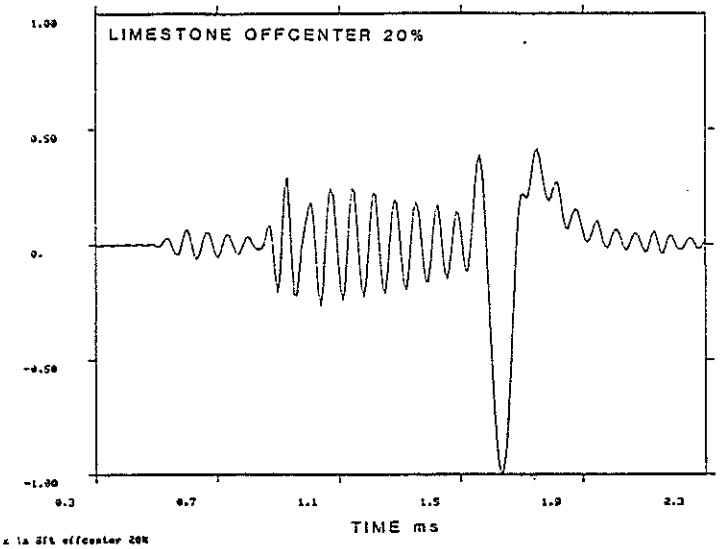

Figure 17. Synthetic limestone waveform for a) centered case, b) 20% off-center.

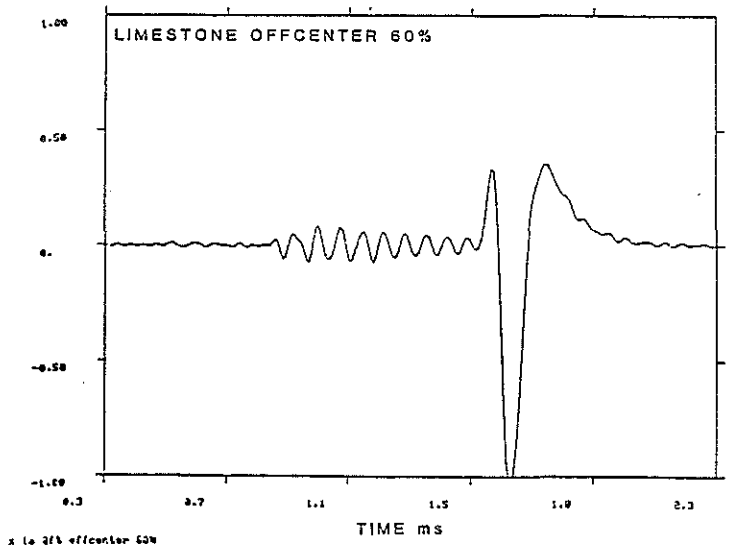

Figure 17c. Synthetic limestone waveform for 60% off-center.

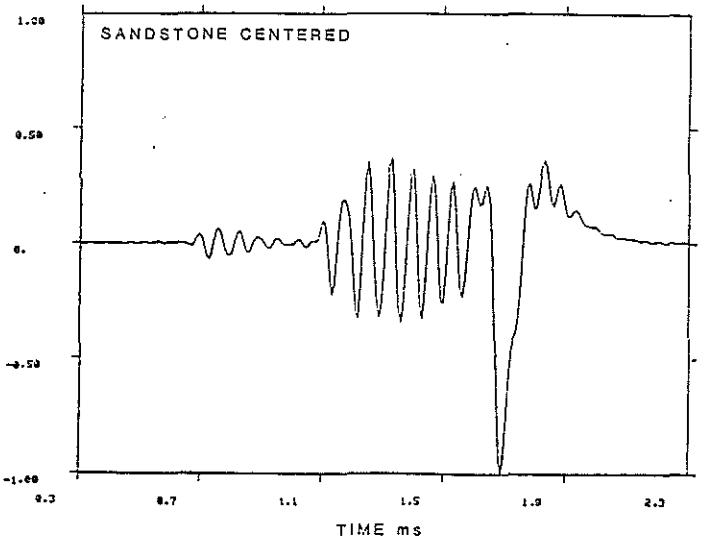

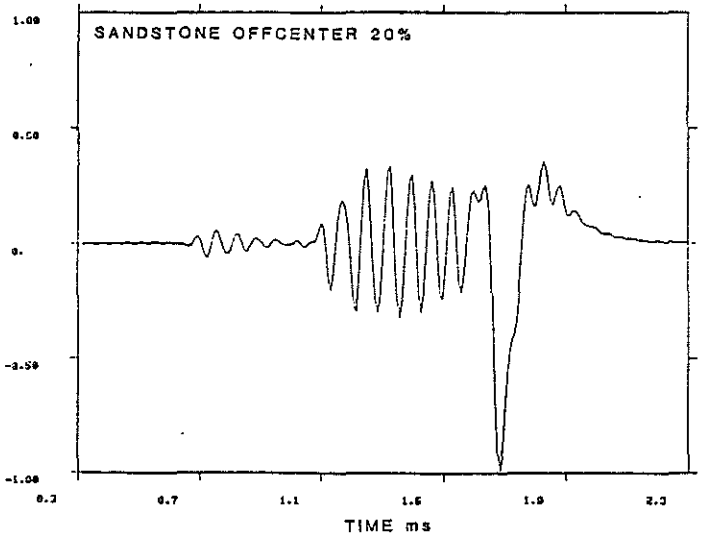

Figure 18. Synthetic sandstone waveform for a) centered case, b) 20% off-center.

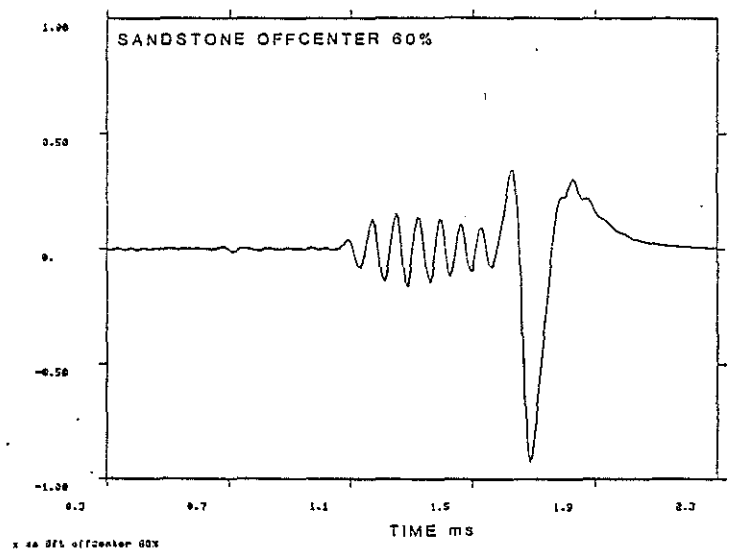

Figure 18c. Synthetic sandstone waveform for 60% off-center.

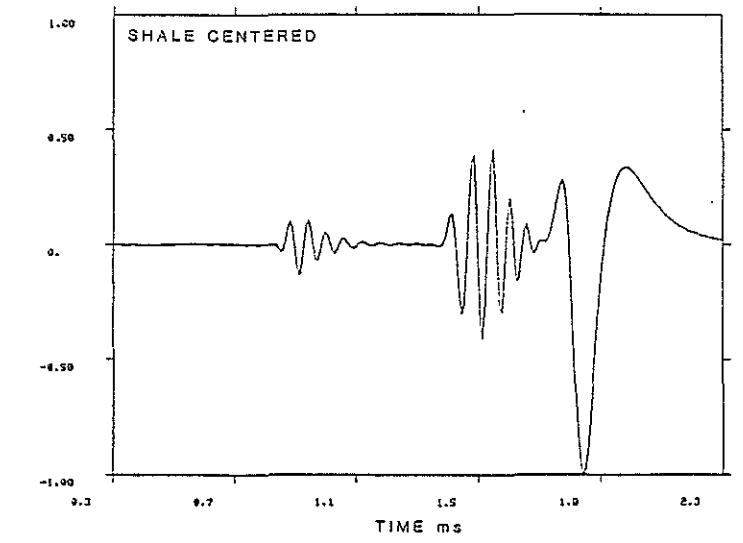

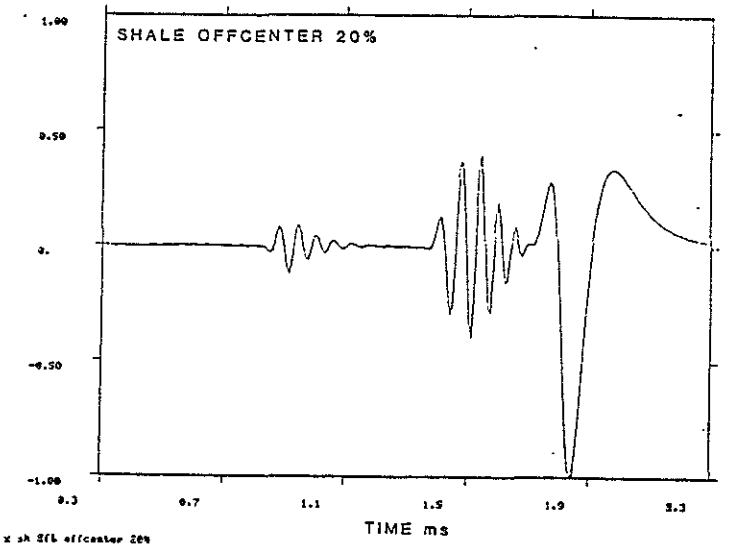

Figure 19. Synthetic shale waveform for a) centered case, b) 20% off-center.

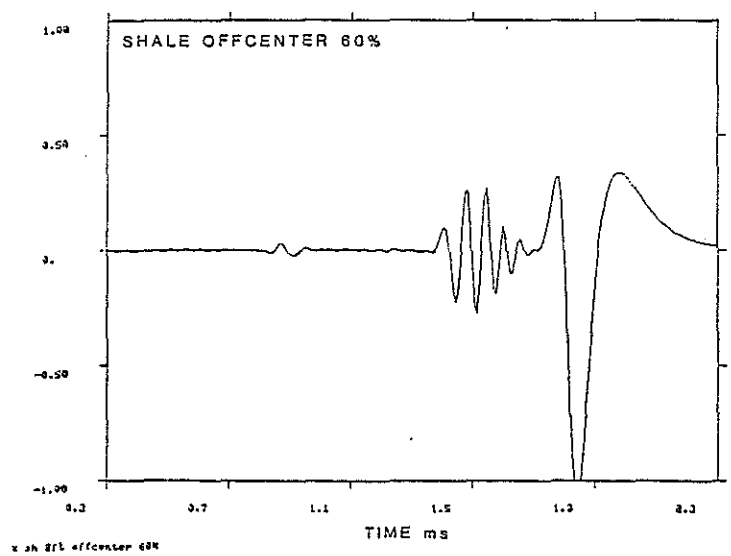

Figure 19c. Synthetic shale waveform for 60% off-center.